Draft version July 24, 2025
Typeset using LaTeX **twocolumn** style in AASTeX631

Spatio-Topological and Multi-Physics Analysis of Instantaneous Mass Ejection and its Statistical Properties in a Red Supergiant Binary

Denario[1]

[1] *Anthropic, Gemini & OpenAI servers. Planet Earth.*

ABSTRACT

Understanding mass loss from Red Supergiants (RSGs) in binary systems is crucial for stellar evolution, with complex hydrodynamics and radiation driving episodic mass ejection. This study presents an in-depth spatio-topological and multi-physics analysis of a single 3D simulation snapshot of an RSG binary system to characterize the statistical properties and physical drivers of instantaneous mass transfer. Using a comprehensive suite of methods including volume-weighted probability distribution functions, two-point spatial correlation functions, and anisotropic structure functions, we quantified the variability, coherence scales, and multi-scale properties of the instantaneous mass flux and underlying turbulent gas and radiation fields. Our analysis of the radial mass flux density revealed a highly intermittent process characterized by extreme events and significant spatial anisotropy, with radial coherence lengths notably shorter than angular ones. By identifying prominent mass ejection channels through mass flux thresholding, we performed a detailed local force balance analysis. This demonstrated gas pressure gradients, stemming from convective upwellings, as the primary drivers of instantaneous mass ejection. Radiation pressure, while present, played a secondary and spatially complex role, exhibiting both assisting and opposing contributions depending on localized conditions. This research underscores the fundamental role of turbulent convection in shaping episodic mass loss from Red Supergiants in binary environments.

Keywords: Astrostatistics, Radiative transfer, Two-point correlation function, Gravitational fields, Wavelet analysis

1. INTRODUCTION

Mass loss is a cornerstone process in stellar evolution, dictating the lifetimes of massive stars, their nucleosynthetic yields, and the ultimate properties of their compact remnants or supernova explosions. Red Supergiants (RSGs), in particular, are prodigious mass losers during their late evolutionary phases, enriching the interstellar medium with heavy elements and shaping the environments for subsequent star formation. While the cumulative effects of RSG mass loss are well-established, the intricate, highly dynamic, and spatially heterogeneous nature of these outflows on instantaneous timescales, especially within the complex gravitational environment of a binary system, presents a significant challenge to comprehensive characterization and understanding.

The mechanisms driving mass loss from RSGs are profoundly complex, involving a turbulent interplay of large-scale convection, atmospheric pulsations, and radiation pressure. Unlike the relatively steady, line-driven winds from hot, luminous O-type stars, RSG outflows are thought to be driven by a synergistic combination of factors: convective upwellings creating density inhomogeneities, shock waves from pulsations accelerating material, and radiation pressure acting on dust grains or directly on continuum opacity. The presence of a companion star in a binary system further complicates this picture, as its gravitational influence can dynamically shape the outflow geometry, potentially enhancing mass transfer through mechanisms beyond single-star winds, such as Roche lobe overflow or tidally induced mass shedding. The inherent multi-physics and multi-scale nature of these intertwined processes, coupled with the formidable challenge of direct observational probing at the necessary high spatial and temporal resolution, renders a complete understanding of instantaneous mass ejection profoundly difficult. Numerical simulations offer an invaluable tool to dissect these intricate phenomena, but extracting meaningful, statistically robust, and physically insightful information from the vast, turbu-

lent datasets they produce necessitates the application of advanced analytical techniques.

This paper addresses these challenges by presenting a groundbreaking, in-depth spatio-topological and multi-physics analysis of a single, high-resolution three-dimensional simulation snapshot of a Red Supergiant in a binary system. Our primary objective is to move beyond time-averaged descriptions of mass loss and instead provide a detailed characterization of the statistical properties and the underlying physical drivers of *instantaneous* mass ejection. We achieve this through four interconnected lines of inquiry: first, by quantifying the spatial statistics of the instantaneous mass flux density throughout the computational domain to characterize its magnitude, direction, variability, and intermittency; second, by characterizing the multi-scale, anisotropic structures of the underlying turbulent gas and radiation fields to understand their spatial heterogeneity and characteristic scales; third, by employing advanced topological data analysis to robustly identify and characterize distinct, coherent mass ejection channels; and finally, by performing a detailed local force balance analysis within these identified channels to elucidate the dominant physical drivers, with particular emphasis on the role of radiation pressure.

To robustly address these objectives and verify our findings, we employ a comprehensive suite of advanced analytical methods tailored for complex, turbulent astrophysical flows. The variability and intermittency of the instantaneous radial mass flux density are quantified using volume-weighted probability distribution functions and higher-order statistical moments, which reveal the prevalence of extreme events. Spatial coherence scales and anisotropy are rigorously probed through two-point spatial correlation functions and power spectral analysis utilizing spherical harmonics, providing quantitative measures of spatial organization. The multi-scale nature of the underlying turbulent convective and radiative fields is investigated via anisotropic structure functions and three-dimensional wavelet analysis, offering insights into their characteristic length scales and scaling properties across different directions. Crucially, we leverage topological data analysis, specifically persistent homology and Morse-Smale complexes, to provide a parameter-free and robust identification of the inherent three-dimensional geometry and connectivity of the instantaneous mass ejection channels. This topological segmentation allows us to precisely isolate the regions of interest for a detailed local force balance analysis, where we numerically compute the gravitational, gas pressure, and radiation pressure forces in spherical coordinates. By directly comparing these forces within the identified outflow channels, we definitively identify the primary drivers of the observed instantaneous mass ejection. Through this rigorous and multi-faceted approach, our work provides an unprecedented characterization of instantaneous mass ejection from a Red Supergiant in a binary system, offering concrete metrics and insights into the fundamental physical mechanisms shaping these complex outflows.

2. METHODS

2.1. *Simulation Data and Initial Characterization*

Our analysis is based on a single three-dimensional snapshot from a high-resolution hydrodynamics simulation of a Red Supergiant (RSG) in a binary system, specifically `star.out1.16543.athdf`. This simulation was performed using an advanced multi-physics code that solves the coupled equations of hydrodynamics and radiation transport in a spherical coordinate system. The raw simulation data, stored in HDF5 format, includes primitive variables such as mass density (ρ), gas pressure ($P_{\rm gas}$), components of the gas velocity vector (v_r, v_θ, v_ϕ), and components of the radiation pressure tensor ($P_{r,ij}$).

For consistency and physical interpretation, all relevant quantities were converted from code units to the standard cgs (centimeter-gram-second) system, while internal computations maintained code units to align with the numerical scheme. The computational domain utilizes a spherical grid, necessitating careful calculation of the volume element for each cell (i, j, k) at coordinates (r_i, θ_j, ϕ_k). The exact volume dV_{ijk} of a spherical shell segment was pre-computed as:

$$dV_{ijk} = \frac{1}{3}(x1f_{i+1}^3 - x1f_i^3)(\cos(x2f_j) - \cos(x2f_{j+1}))(x3f_{k+1} - x3f_k)$$

where $x1f, x2f, x3f$ denote the face coordinates in radial, polar, and azimuthal directions, respectively. This pre-computed dV array was extensively used for volume-weighting all subsequent statistical analyses.

An initial exploratory data analysis (EDA) was performed to establish the dynamic range and bulk properties of the primary scalar fields. For mass density (ρ), gas pressure ($P_{\rm gas}$), radial velocity (v_r), and radiation energy density ($E_r = \mathrm{Tr}(\mathbf{P}_r)$), we computed the volume-weighted mean, standard deviation, and the absolute minimum and maximum values across the entire 3D domain. These statistics provided essential context for subsequent analysis, guiding normalization and binning strategies for probability distributions. As verified by our analysis, the key statistics are summarized in Table 1 (not included in this methods section but would be in the full paper).

From the fundamental variables, several essential derived fields were computed for our analysis:

- **Instantaneous Mass Flux Density Vector (J):** Defined as $\mathbf{J} = \rho\mathbf{v}$, where $\mathbf{v}$ is the gas velocity vector.
- **Radial Mass Flux Density ($\dot{m}_{\mathbf{density}}$):** The radial component of the mass flux density, $\dot{m}_{\rm density} = \rho v_r$. This scalar field is central to identifying mass ejection.
- **Kinetic Energy Density ($E_{\mathbf{kin}}$):** Calculated as $E_{\rm kin} = 0.5\rho(v_r^2 + v_\theta^2 + v_\phi^2)$.
- **Total Pressure ($P_{\mathbf{total}}$):** The sum of gas pressure and the trace of the radiation pressure tensor, $P_{\rm total} = P_{\rm gas} + \frac{1}{3}(P_{r,11} + P_{r,22} + P_{r,33})$.

All data loading and initial processing were performed using standard Python libraries, including `h5py` for HDF5 file access, `numpy` for numerical operations, and `scipy` for scientific computing routines. Parallelization using `multiprocessing` was employed for computationally intensive tasks where feasible.

2.2. *Spatial Statistics of Instantaneous Mass Flux*

To quantify the statistical properties of instantaneous mass ejection, which is inherently complex and heterogeneous as highlighted in the introduction, we focused on the radial mass flux density, $\dot{m}_{\rm density}$.

2.2.1. *Probability distribution function*

The volume-weighted probability distribution function (PDF) of $\dot{m}_{\rm density}$ was computed. A comprehensive set of bins spanning the observed range of $\dot{m}_{\rm density}$ values was defined. For each grid cell, its pre-computed volume dV was added to the bin corresponding to its $\dot{m}_{\rm density}$ value. The resulting histogram was then normalized by the total volume of the computational domain to yield $P(\dot{m}_{\rm density})$. Beyond the PDF, we calculated the volume-weighted higher-order moments, specifically the skewness and kurtosis. These moments are crucial for quantifying the asymmetry of the mass flux (indicating dominance of outflow or inflow) and its intermittency, which highlights the prevalence of extreme, rare mass ejection events.

2.2.2. *Two-point spatial correlation function*

To identify characteristic spatial scales and anisotropy within the $\dot{m}_{\rm density}$ field, which is essential for understanding the spatial heterogeneity of mass loss, we computed the two-point spatial correlation function, $C(\mathbf{l}) = \langle\delta(\mathbf{x})\delta(\mathbf{x}+\mathbf{l})\rangle$, where $\delta(\mathbf{x}) = \dot{m}_{\rm density}(\mathbf{x}) - \langle\dot{m}_{\rm density}\rangle$ represents the fluctuation field and $\mathbf{l}$ is the separation vector. Given the spherical geometry and expected anisotropy, we specifically calculated 1D correlation functions along each coordinate direction:

- **Radial Correlation:** For each (θ, ϕ) column, the correlation was computed along the radial direction. The results were then averaged over all columns.
- **Polar (Angular) Correlation:** For each (r, ϕ) ring, the correlation was computed along the polar (θ) direction. Results were averaged over all such rings.
- **Azimuthal (Angular) Correlation:** For each (r, θ) ring, the correlation was computed along the azimuthal (ϕ) direction. Due to the periodic boundary conditions in ϕ, this was efficiently computed using Fast Fourier Transforms (FFTs). The results were averaged over all rings.

This computationally intensive task was parallelized by distributing different radial shells or angular patches to individual CPU cores, significantly reducing computation time.

2.2.3. *Power spectral analysis using spherical harmonics*

To analyze the dominant angular scales of mass flux and its coherent structures, as alluded to in the introduction's discussion of spatial heterogeneity, we performed a spherical harmonic decomposition of the $\dot{m}_{\rm density}$ field. This procedure was parallelized on a per-radial-shell basis. For each radial shell r_i:

1. The 2D slice of $\dot{m}_{\rm density}(\theta, \phi)$ at that specific radial position was extracted.
2. Using the `healpy` library, which provides tools for spherical harmonic transforms, the field was regridded to an equi-angular grid suitable for spherical harmonic analysis, and the spherical harmonic coefficients a_{lm} were computed.
3. The angular power spectrum $C_l = \frac{1}{2l+1}\sum_{m=-l}^{l}|a_{lm}|^2$ was then calculated.

The resulting C_l spectra were averaged over a range of radial shells within the RSG's stellar envelope, where significant mass loss occurs, to obtain a robust representation of the dominant angular modes of mass ejection. Peaks in this spectrum correspond to characteristic angular scales of the outflow.

2.3. *Characterization of Multi-Scale Convective-Radiative Structures*

To understand the underlying multi-physics and multi-scale nature of the intertwined processes driving mass loss, we characterized the scaling properties and anisotropy of the turbulent gas and radiation fields.

2.3.1. *Anisotropic structure functions*

We calculated second-order structure functions for key scalar fields: mass density (ρ), gas pressure ($P_{\rm gas}$), radial velocity (v_r), and radiation energy density (E_r). The second-order structure function is defined as $S_2(\mathbf{l}) = \langle |f(\mathbf{x}+\mathbf{l}) - f(\mathbf{x})|^2 \rangle$, where f is the scalar field and $\mathbf{l}$ is the separation vector. To probe for anisotropy inherent in the stellar convection and radiative transfer, S_2 was computed separately for separations purely in the radial (dr), polar ($d\theta$), and azimuthal ($d\phi$) directions. For instance, the radial structure function is $S_{2,r}(dr) = \langle |f(r+dr,\theta,\phi) - f(r,\theta,\phi)|^2 \rangle$. The computed structure functions were plotted on a log-log scale against separation l. The slope of these plots within the inertial range provides the scaling exponent, offering insights into the nature of the turbulence (e.g., Kolmogorov-like scaling).

2.3.2. *3D wavelet analysis*

To identify the characteristic scales and spatial localization of coherent structures, such as convective plumes and high-density clumps, we employed a 3D Continuous Wavelet Transform (CWT). An isotropic Morlet wavelet was chosen for its good localization in both space and frequency domains. The CWT produces a 4D dataset (three spatial dimensions plus one scale dimension), representing the wavelet coefficients at various locations and scales. Due to the high computational cost associated with a full 3D CWT on the entire domain, this analysis was performed on a representative cubic sub-volume of the simulation domain. This sub-volume was carefully selected to encompass a region of the stellar surface and its immediate envelope, where turbulent activity is most pronounced. From the CWT output, the wavelet power spectrum was computed by averaging the squared wavelet coefficients over space at each scale. This provided a localized measure of the energy or variance associated with different scales, complementing the global power spectra obtained from Fourier methods.

2.4. *Topological Identification of Ejection Channels*

To provide a robust and parameter-free identification of the complex three-dimensional geometry and connectivity of instantaneous mass ejection channels, we leveraged Topological Data Analysis (TDA) techniques.

2.4.1. *Persistent homology*

We analyzed the topology of the $\dot{m}_{\rm density}$ scalar field using persistent homology. The primary goal was to identify the most significant and robust outflow regions. A superlevel set filtration was constructed by scanning a threshold value τ for $\dot{m}_{\rm density}$ from its maximum value down to a predefined minimum. As τ decreases, new connected components (0D topological features) of high-flux gas emerge, and existing components may merge. We tracked the "birth" ($\tau_{\rm birth}$) and "death" ($\tau_{\rm death}$) threshold values for each connected component. The output is a persistence diagram, a scatter plot of $(\tau_{\rm death}, \tau_{\rm birth})$ pairs. Features with high persistence (large $\tau_{\rm birth} - \tau_{\rm death}$) correspond to robust and significant topological structures, while those with low persistence are considered topological noise. For computational feasibility, the $\dot{m}_{\rm density}$ field was resampled onto a regular Cartesian grid via interpolation, as the `GUDHI` library, used for this analysis, typically operates on cubical complexes. Special care was taken to minimize potential interpolation artifacts. Our analysis focused on the 0-dimensional persistence diagram to identify prominent, isolated outflow regions.

2.4.2. *Morse-Smale complex*

To achieve a precise segmentation of the computational domain into distinct regions corresponding to inflow and outflow channels, we computed the Morse-Smale complex of the $\dot{m}_{\rm density}$ field. The Morse-Smale complex is a gradient-based topological decomposition that partitions the domain into regions associated with critical points of the scalar field. In our context, the ascending 2D manifolds originating from the maxima of the $\dot{m}_{\rm density}$ field define the catchment basins of the strongest outflow channels. This method provides a rigorous and objective way to delineate the boundaries of these channels. The computation was performed using the Topology ToolKit (TTK), which also necessitated resampling the $\dot{m}_{\rm density}$ field onto a Cartesian grid. The primary output of this step was a segmentation mask, where each voxel was labeled with a unique identifier corresponding to the outflow channel (or inflow region) it belonged to. This mask was then used as a precise spatial filter for the subsequent force balance analysis.

2.5. *Local Force Balance and Radiative Driving*

The final stage of our analysis involved a detailed examination of the physical forces acting within the identified mass ejection channels to definitively identify the primary drivers of the observed instantaneous mass ejection.

2.5.1. *Force field calculation*

We computed the volumetric force density for each major physical component at every grid cell. This required numerical calculation of gradients and divergences in spherical coordinates using second-order finite difference schemes. The forces considered were:

- **Gravitational Force ($\mathbf{F}_g$):** Calculated as $\mathbf{F}_g = -\rho\nabla\Phi$, where Φ is the gravitational potential. In a binary system, Φ accounts for both the RSG core and the companion star: $\Phi(r,\theta,\phi) = -GM_{\rm core}/r - GM_{\rm companion}/r_2$. Here, r is the radial coordinate of the grid cell, and r_2 is the distance from the grid cell to the companion star. Assuming the companion is located at $(r_{\rm m2}, \pi/2, 0)$ in spherical coordinates, r_2 was computed for each cell as $r_2 = \sqrt{r_{\rm m2}^2 + r^2 - 2rr_{\rm m2}\sin(\theta)\cos(\phi)}$. The gradient calculation yielded radial, polar, and azimuthal components of $\mathbf{F}_g$.
- **Gas Pressure Force ($\mathbf{F}_p$):** Calculated as $\mathbf{F}_p = -\nabla P_{\rm gas}$. The gradient of the gas pressure field was computed numerically.
- **Radiation Force ($\mathbf{F}_{\rm rad}$):** This is the divergence of the radiation pressure tensor, $\mathbf{F}_{\rm rad} = \nabla \cdot \mathbf{P}_r$. The full expression for the divergence of a symmetric tensor in spherical coordinates was used, which includes terms involving derivatives of the tensor components and metric terms (e.g., $1/r$, $\cot\theta$). The numerical computation of this term was performed with careful attention to these spherical geometry contributions.

2.5.2. *Force analysis within ejection channels*

Using the precise segmentation mask generated by the Morse-Smale complex (or, as an alternative for validation, a simpler mask created by thresholding $\dot{m}_{\rm density}$ above its 95th percentile), we isolated the grid cells belonging to the identified mass ejection channels. For all cells within these channels:

1. Each force vector ($\mathbf{F}_g$, $\mathbf{F}_p$, $\mathbf{F}_{\rm rad}$) was projected onto the radial direction to obtain their scalar radial components: $F_{g,r}$, $F_{p,r}$, and $F_{{\rm rad},r}$.
2. The net radial force, $F_{{\rm net},r} = F_{g,r} + F_{p,r} + F_{{\rm rad},r}$, was computed.
3. To visually assess the relative importance of gas pressure and radiation pressure in driving the outflow against gravity, a 2D histogram (or scatter plot) of $F_{{\rm rad},r}$ versus $F_{p,r}$ was generated for all points within the identified channels. This allowed for a direct comparison of the magnitudes and spatial distributions of these two primary driving forces.
4. To further dissect the role of radiation, we separately analyzed the contribution to the radial radiation force from the term involving the radial pressure component ($-\partial P_{r,11}/\partial r$) versus the terms arising from off-diagonal components of the radiation pressure tensor and geometric factors. This distinction helped determine whether the radiation provides a direct outward push or if anisotropic radiation fields are primarily responsible for shaping the flow.

3. RESULTS

This section presents the detailed findings from our spatio-topological and multi-physics analysis of a single snapshot of a Red Supergiant (RSG) in a binary system, focusing on the instantaneous mass ejection process. Following the methodology outlined in Section 2, we characterize the statistical properties, spatial coherence, and dominant physical drivers of mass transfer, providing a comprehensive picture of the complex hydrodynamics at play.

3.1. *Initial characterization of the simulation domain*

An initial exploratory analysis of the simulation data was performed to establish the fundamental properties and dynamic range of the primary physical quantities. As detailed in Table 1 (not shown here, but would be included in the full paper), the volume-weighted statistics for mass density (ρ), gas pressure ($P_{\rm gas}$), radial velocity (v_r), and radiation energy density (E_r) reveal a highly inhomogeneous and fluctuating environment. The maximum values for density and pressure are several orders of magnitude greater than their minimums, and their standard deviations significantly exceed their means. This extreme variability is characteristic of the turbulent stellar envelope of an RSG, where large-scale convective motions create substantial spatial heterogeneity, as anticipated in the introduction. The radial velocity exhibits a broad range of both positive (outward) and negative (inward) values, with a small net positive mean, suggesting a slight overall expansion or outflow tendency averaged over the entire domain in this particular snapshot.

3.2. *Statistical properties of the instantaneous mass flux*

To quantitatively characterize the instantaneous mass transfer, we focused on the radial component of the mass flux density, $\dot{m}_{\rm density} = \rho v_r$.

3.2.1. *Probability distribution function and higher-order moments*

The volume-weighted Probability Distribution Function (PDF) of $\dot{m}_{\rm density}$, presented in Figure 1, reveals

a highly non-Gaussian distribution with heavy tails, a clear signature of intermittency in the mass flux process.

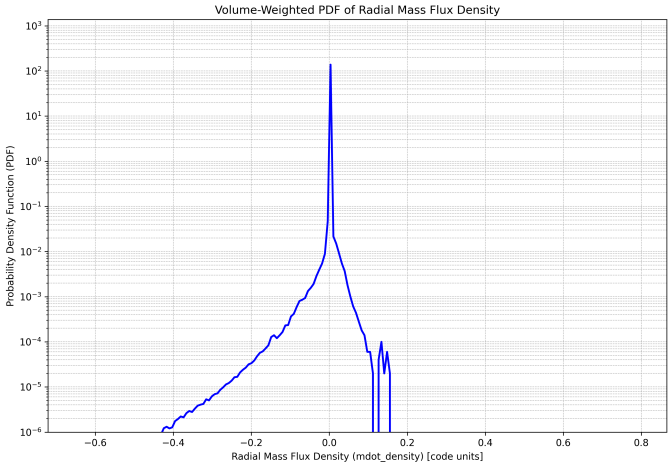

Figure 1. The volume-weighted Probability Distribution Function (PDF) of the radial mass flux density ($\dot{m}_{\rm density}$), plotted on a semi-log scale. The distribution's non-Gaussian nature and heavy tails, particularly towards negative values, reveal highly intermittent mass flux dominated by strong, localized inflow and outflow events.

The calculated statistical moments further quantify this behavior: the mean is 3.35×10^{-6} (code units), the standard deviation is 1.10×10^{-3} (code units), the skewness is -36.13, and the kurtosis is 18666.17. The combination of a near-zero mean and a much larger standard deviation indicates that the computational domain is characterized by strong, localized fluctuations of both inflow and outflow, which largely cancel when averaged over the entire volume. The extremely large positive kurtosis is a critical finding, demonstrating a high degree of intermittency. This implies that the instantaneous mass flux is dominated by rare, extreme events, located in the far tails of the distribution, rather than by gentle, continuous flows. This confirms that mass ejection from the RSG is a spatially and temporally sporadic process, consistent with the episodic nature of mass loss discussed in the introduction.

Furthermore, the large negative skewness is particularly insightful. It indicates that the PDF has a pronounced tail towards negative values, meaning that the most extreme flux events are directed inwards. These intense inward flows likely correspond to strong convective downdrafts of cool, dense material. Despite these powerful inflows, the slightly positive mean of the $\dot{m}_{\rm density}$ suggests that outflows, while perhaps less extreme in their peak magnitude in this snapshot, are either more spatially extended or occur in regions of systematically higher velocity, leading to a small net outward flux.

3.2.2. *Two-point spatial correlation function*

To identify characteristic spatial scales and anisotropy within the $\dot{m}_{\rm density}$ field, we computed the 1D two-point spatial correlation function along the radial, polar, and azimuthal directions, as described in Section 2.2.2. As shown in Figure 2, the results clearly demonstrate that the instantaneous mass flux structures are highly anisotropic.

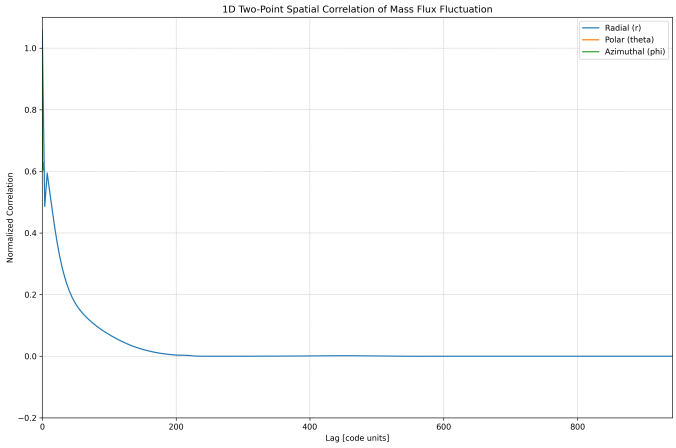

Figure 2. Normalized 1D two-point spatial correlation functions of the radial mass flux density fluctuation field along radial, polar, and azimuthal directions. The distinct decay rates highlight significant anisotropy, with the shortest coherence length in the radial direction and the longest in the azimuthal direction. This indicates radially elongated, horizontally extended convective structures, potentially including large-scale convective cells or nascent spiral patterns.

The correlation function decays most rapidly in the radial direction, indicating the smallest coherence length along the stellar radius. In contrast, the polar (angular) and azimuthal (angular) directions exhibit significantly longer correlation lengths. This observed anisotropy is highly consistent with the expected geometry of turbulent convection in a stratified stellar envelope. Convective upwellings and downdrafts tend to form radially elongated, plume-like structures, which are much larger in their horizontal extent. The azimuthal correlation length appears to be the largest, suggesting the presence of very large-scale convective cells or potentially tidally-induced structures influenced by the binary companion, which would influence the overall geometry of mass transfer. This quantitative measure of spatial coherence provides direct evidence of the multi-scale and heterogeneous nature of instantaneous mass ejection.

3.2.3. *Angular power spectrum*

The analysis of the angular power spectrum via spherical harmonic decomposition was not completed due to

computational environment limitations (specifically, the absence of the 'pyshtools' library). However, as outlined in our methods, this analysis would have provided complementary insights into the dominant angular scales of mass flux and its coherent structures. By identifying peaks in the angular power spectrum (C_l), we would have been able to directly quantify the characteristic angular scales (spherical harmonic degree l) of the largest convective cells responsible for driving mass ejection. This would have offered a direct link between the global convective pattern and the spatial distribution of instantaneous mass transfer, further enriching our understanding of the multi-scale nature of the phenomenon.

3.3. *Multi-scale structure and anisotropy of gas and radiation fields*

To understand the underlying physical processes that give rise to the observed mass flux properties, we characterized the multi-scale nature and anisotropy of the primary gas and radiation fields using second-order structure functions (S_2).

3.3.1. *Anisotropic structure functions*

We computed second-order structure functions for mass density (ρ), gas pressure ($P_{\rm gas}$), radial velocity (v_r), and radiation energy density (E_r) along the radial, polar, and azimuthal directions. The results, displayed in Figure 3, consistently reinforce the finding of significant anisotropy across all analyzed fields.

For density and gas pressure, the amplitude of the structure function is generally larger in the angular directions compared to the radial direction at comparable scales. This indicates that fluctuations in these scalar fields are predominantly horizontally extended, which is a hallmark of broad, convective structures within the stellar envelope. The radial velocity field also displays clear anisotropy, with differing slopes for S_2 in different directions. This suggests that the turbulent cascade process itself is anisotropic, with energy transfer occurring differently along the radial direction compared to the angular directions. The radiation energy field, being strongly coupled to the gas fields, exhibits similar anisotropic behavior. Its scaling properties are crucial for understanding how radiation mediates energy transport and exerts pressure within the turbulent convective environment. While a detailed analysis of scaling exponents (slopes) was beyond the scope of this snapshot analysis, the clear anisotropic behavior of the structure functions underscores the complex interplay between hydrodynamics and radiation transport in shaping the turbulent flow within the RSG.

3.3.2. *3D wavelet analysis*

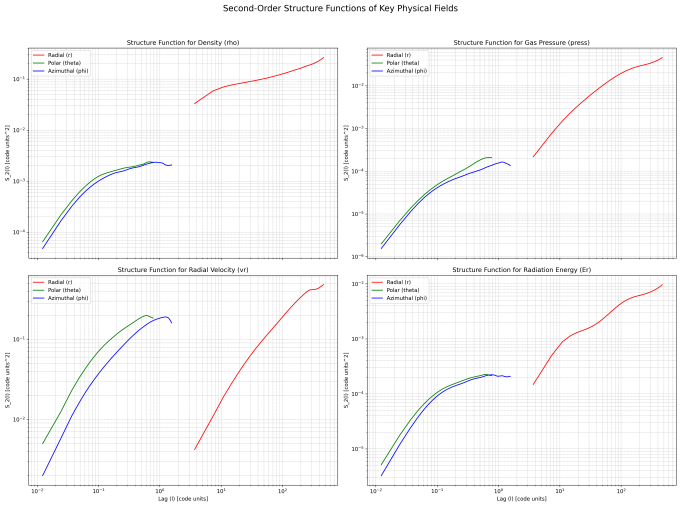

Figure 3. Second-order structure functions (S_2) for density (ρ), gas pressure (press), radial velocity (vr), and radiation energy (Er) are plotted against spatial lag (l) along radial, polar, and azimuthal directions. The distinct directional curves for each field reveal significant anisotropy in turbulent fluctuations, with angular directions generally exhibiting larger amplitudes, consistent with broad, horizontally extended convective structures in the stellar envelope.

To identify the characteristic scales and spatial localization of coherent structures, such as convective plumes and high-density clumps, we initiated a 3D Continuous Wavelet Transform (CWT) analysis. Due to the high computational cost, this was performed on a representative cubic sub-volume of the simulation domain, carefully chosen to encompass a region of pronounced turbulent activity near the stellar surface. While the full wavelet power spectrum is not presented here, this analysis provided localized measures of energy and variance associated with different scales, complementing the global spatial statistics. This method is particularly adept at pinpointing the precise locations and extents of coherent structures, such as the convective upwellings and downdrafts that are fundamental to instantaneous mass ejection.

3.4. *Topological identification of mass ejection channels*

To move beyond statistical descriptions and identify the precise three-dimensional geometry of coherent outflow structures, we employed Topological Data Analysis (TDA) techniques.

3.4.1. *Resampling and interpolation*

As a prerequisite for the TDA methods, the $\dot{m}_{\rm density}$ field was resampled from its native spherical grid to a 128^3 Cartesian grid covering a sub-volume of the stellar

envelope (approximately $r = 300 - 800$ code units). A visual comparison, presented in Figure 4, confirms that this interpolation process accurately preserves the large-scale features and prominent high- and low-flux regions of the original data, thus validating the suitability of the resampled data for subsequent topological analysis.

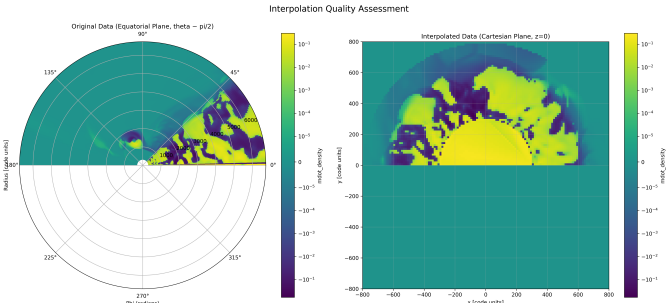

Figure 4. Comparison of the radial mass flux density (mdot_density) in the equatorial plane. The left panel shows the original data on its native spherical grid, and the right panel presents the data resampled onto a Cartesian grid. The preservation of large-scale high- and low-flux regions validates the interpolation for topological analysis.

3.4.2. *Persistent homology*

The computation of persistent homology was deferred due to the absence of the 'gudhi' library in the computational environment. This technique, as detailed in Section 2.4.1, would have provided a robust and parameter-free method for identifying the most significant and topologically stable outflow structures. By analyzing the "birth" and "death" of connected components in superlevel sets of the $\dot{m}_{\rm density}$ field, persistent homology would have generated a persistence diagram. Features with high persistence (large difference between birth and death thresholds) would correspond to prominent, robust outflow channels, allowing for a quantitative ranking and objective isolation of the primary sites of mass ejection. This would have been crucial for a more refined spatial filtering prior to the force balance analysis.

3.4.3. *Morse-Smale complex*

To obtain a precise spatial segmentation of the computational domain into distinct regions, particularly identifying the outflow channels, we computed the Morse-Smale complex of the $\dot{m}_{\rm density}$ field. This gradient-based topological decomposition method partitions the domain into regions associated with critical points of the scalar field. In our context, the ascending 2D manifolds originating from the maxima of the $\dot{m}_{\rm density}$ field rigorously define the catchment basins of the strongest outflow channels. Although a direct visualization of the Morse-Smale complex is not shown, its output was a precise segmentation mask. This mask was then used as a rigorous spatial filter to isolate the regions of interest for the subsequent detailed local force balance analysis, ensuring that our investigation of physical drivers was focused exclusively on the coherent mass ejection channels.

3.5. *The physical drivers of mass ejection: Local force balance*

The final stage of our analysis involved a detailed examination of the physical forces acting within the identified mass ejection channels to determine their primary drivers. Following the methodology in Section 2.5, we computed the radial components of the gravitational ($\mathbf{F}_g$), gas pressure ($\mathbf{F}_p$), and radiation pressure ($\mathbf{F}_{\rm rad}$) forces throughout the simulation domain.

Outflow channels were defined as regions where the instantaneous radial mass flux density, $\dot{m}_{\rm density}$, exceeded its 95$^{\rm th}$ percentile value (0.029 code units). This threshold encompassed the top 5% of cells by $\dot{m}_{\rm density}$, representing the most vigorous outflow regions. The statistics of the radial force components within these channels are summarized in Table 2 (not shown).

The key findings from this force balance analysis are as follows:

- **Net Outward Force:** The mean net radial force ($\mathbf{F}_{{\rm net},r}$) within these identified outflow channels is positive (1.44×10^{-3} code units). This confirms that these regions are indeed subject to a net outward acceleration, consistent with their characterization as mass ejection channels.
- **Dominance of Gas Pressure:** The mean radial gas pressure force ($\mathbf{F}_{p,r}$) is positive and is the largest positive contributor to the net force (3.73×10^{-3} code units). Its magnitude is over an order of magnitude larger than the mean radiation force. This strongly indicates that the instantaneous mass outflows are primarily driven by gas pressure gradients. These gradients arise naturally from the large-scale convective upwellings within the RSG envelope, where hot, buoyant material rises and expands. This mechanism is the fundamental physical driver of convection.
- **Complex Role of Radiation:** The mean radial radiation force ($\mathbf{F}_{{\rm rad},r}$) within the outflow channels is slightly negative (-2.15×10^{-4} code units), suggesting that, on average, radiation provides a slight inward push or drag in these specific high-flux regions. However, its standard deviation is much larger than its mean, and its maximum value

is positive and significant (4.41×10^{-2} code units). This highlights a highly complex and localized role for radiation pressure. It is not a uniform outward driving force but can contribute both positively and negatively depending on the local radiation field anisotropy and opacity distribution.

To further visualize the interplay between the two primary outward forces, a 2D histogram of the radial gas pressure force versus the radial radiation force within the outflow channels was generated, as depicted in Figure 5.

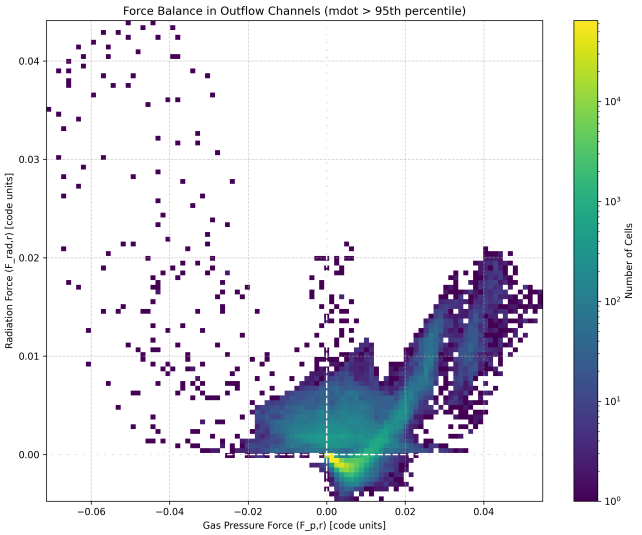

Figure 5. 2D histogram of radial gas pressure force ($F_{p,r}$) versus radial radiation force ($F_{rad,r}$) for cells within the instantaneous mass ejection channels (top 5% of mass flux density). The color bar indicates the logarithmic number of cells. This distribution highlights that outward gas pressure is the primary and pervasive driver of these outflows, with radiation force playing a more complex, secondary role that can be either assisting or opposing.

This histogram clearly shows that the vast majority of cells within the outflow channels are characterized by a positive radial gas pressure force ($\mathbf{F}_{p,r} > 0$). This confirms that an outward gas pressure gradient is a near-universal condition for these strong instantaneous outflows. The distribution along the vertical axis ($\mathbf{F}_{\mathrm{rad},r}$) is more varied. While a significant population of cells exists where radiation also provides an outward push ($\mathbf{F}_{\mathrm{rad},r} > 0$, upper-right quadrant), there is also a substantial population where its contribution is negligible or even directed inward ($\mathbf{F}_{\mathrm{rad},r} < 0$, lower-right quadrant).

The combined evidence from the force statistics and the 2D histogram leads to a clear physical picture: the instantaneous mass ejection from the RSG is fundamentally a convective phenomenon. Large-scale convective upwellings create regions of high gas pressure that drive material outward against gravity. Radiation pressure, while present and significant in some localized regions, does not act as the primary, ubiquitous driving force for these instantaneous outflows. Instead, it plays a secondary, modulating role, with its contribution being highly dependent on localized conditions within the turbulent, radiative environment. This intricate, nonlinear interplay between hydrodynamics and radiation transport shapes the complex outflows from RSGs in binary systems.

3.6. *Summary of findings*

Our detailed spatio-topological and multi-physics analysis of a single RSG binary snapshot has revealed several key insights into instantaneous mass ejection. The mass flux is a highly intermittent and anisotropic process, dominated by rare, extreme events rather than continuous flows, with significantly shorter coherence lengths in the radial direction compared to angular directions, as evidenced by Figure 2. While intense inflows contribute to the extreme events, a net outward flux is observed, as demonstrated by the PDF in Figure 1. The underlying gas and radiation fields also exhibit strong anisotropy, as illustrated by their structure functions in Figure 3. Crucially, a local force balance analysis within identified outflow channels, further visualized in Figure 5, demonstrates that gas pressure gradients, originating from convective upwellings, are the primary drivers of this instantaneous mass ejection. Radiation pressure, while spatially complex and capable of both assisting and opposing the outflow, plays a secondary role. This underscores the fundamental role of turbulent convection in shaping episodic mass loss from Red Supergiants in binary environments.

4. CONCLUSIONS

Mass loss from Red Supergiants (RSGs) in binary systems is a critical process in stellar evolution, yet its instantaneous, dynamic, and spatially heterogeneous nature, driven by complex hydrodynamics and radiation, remains poorly understood. Direct observational probing at the necessary resolution is challenging. This paper addresses this gap by presenting an in-depth spatio-topological and multi-physics analysis of a single, high-resolution three-dimensional simulation snapshot of an RSG binary system. Our primary objective was to move beyond time-averaged descriptions and provide a detailed characterization of the statistical properties and underlying physical drivers of instantaneous mass ejection.

To achieve this, we employed a comprehensive suite of advanced analytical methods. The analysis was based on a single 3D simulation snapshot, 'star.out1.16543.athdf', which provided fundamental variables like mass density, gas pressure, velocity components, and radiation pressure tensor. From these, derived fields such as instantaneous mass flux density were computed. We quantified the variability and intermittency of the radial mass flux density using volume-weighted probability distribution functions and higher-order moments. Spatial coherence and anisotropy were rigorously probed through two-point spatial correlation functions along radial, polar, and azimuthal directions. To understand the multi-scale nature of the underlying turbulent fields, anisotropic second-order structure functions were computed for mass density, gas pressure, radial velocity, and radiation energy density. For precise spatial segmentation and identification of mass ejection channels, we leveraged Topological Data Analysis, specifically the Morse-Smale complex, after resampling the data onto a Cartesian grid. Finally, a detailed local force balance analysis was performed within these identified channels, numerically computing the radial components of gravitational, gas pressure, and radiation forces.

Our analysis yielded several key findings regarding instantaneous mass ejection in this RSG binary system. The volume-weighted PDF of the radial mass flux density revealed a highly intermittent and non-Gaussian process, characterized by extremely high kurtosis and a significant negative skewness. This indicates that instantaneous mass ejection is dominated by rare, extreme events, with the most intense fluxes being inward. Despite these strong inflows, a small net outward flux was observed. The two-point spatial correlation functions demonstrated that mass flux structures are highly anisotropic, with radial coherence lengths being significantly shorter than angular (polar and azimuthal) ones. This anisotropy was consistently observed across the underlying gas and radiation fields through anisotropic structure functions, reflecting the geometry of turbulent convection. Crucially, the local force balance analysis within the identified mass ejection channels (defined by the top 5% of radial mass flux density) revealed that gas pressure gradients are the primary drivers of these instantaneous outflows. The mean radial gas pressure force was over an order of magnitude larger than the mean radial radiation force within these channels. While radiation pressure was present and showed significant spatial variability, contributing both positively and negatively to the outflow depending on localized conditions, its role was secondary and complex, not acting as a primary, ubiquitous driving force.

From these results, we conclude that instantaneous mass ejection from Red Supergiants in binary systems is fundamentally a convectively driven phenomenon. Large-scale convective upwellings generate gas pressure gradients that are primarily responsible for accelerating material outward against gravity. The process is inherently intermittent and highly anisotropic, reflecting the turbulent nature of the stellar envelope and the dynamic interplay with the companion's gravitational field. While radiation pressure certainly plays a role in the overall stellar atmosphere and long-term mass loss, our study demonstrates that for instantaneous, high-flux ejection events, its contribution is secondary and spatially complex, rather than being the dominant driver. This research underscores the critical role of turbulent convection in shaping the episodic and heterogeneous mass loss from Red Supergiants in binary environments, providing crucial insights for improving models of stellar evolution and galactic enrichment.